JMEPEG (2012) 21:1046–1050
DOI: 10.1007/s11665-011-9950-z

1059-9495/$19.00

Preparation and Thermal Conductivity of $Dy_2Ce_2O_7$ Ceramic Material

Zhang Hongsong, Liao Suran, and Guan Shaokang

(Submitted November 13, 2010; in revised form April 10, 2011)

$Dy_2Ce_2O_7$ ceramic material was prepared by solid reaction method at 1600 °C for 10 h. The phase composition, microstructure, and thermal conductivity of this material were investigated. XRD results reveal that single-phase $Dy_2Ce_2O_7$ with fluorite structure was synthesized successfully. Microstructure of $Dy_2Ce_2O_7$ was dense and no other unreacted oxides or interphase existed in the interfaces between grains. Because of phonon scattering by oxygen vacancies and difference in atomic mass between substitutional atoms and host atoms, thermal conductivity of $Dy_2Ce_2O_7$ is lower than that of 8YSZ, which implies that this ceramic can be used as novel candidate materials for thermal barrier coatings in the future.

Keywords Ceramic material, Thermal barrier coatings, Thermal conductivity, Phonon scattering

1. Introduction

Thermal barrier coatings (TBCs) of partly Y_2O_3-stabilized ZrO_2 (PYSZ) films are widely used to protect hot section parts of advanced turbines (Ref 1). Their continued development is essential for improving the efficiency and performance of gas turbines by allowing the inlet gas temperature to be increased further (Ref 2). However, zirconate-based ceramic is limited to applications below 1200 °C due to its sintering resistance and phase structure stability during long-term service (Ref 3, 4). In order to further increase the operating efficiency, it is urgently needed to develop new thermal barrier coating materials with a significantly lower thermal conductivity than YSZ for further improvements in engine's performance to increase gas inlet temperatures to 1650 °C or higher. Two important groups of candidate materials, one based on the co-doped of yttria-stabilized zirconia (YSZ) with one or more metal oxides and the other on the rare-earth zirconate ceramics, have been developed for advanced gas-turbine engines, which are intended to operate at temperatures as high as possible (Ref 5, 6).

The rare earth zirconates with general formula $Ln_2Zr_2O_7$ (Ln = rare earth elements) with pyrochlore structures or defect fluorite-type structures show promising thermophysical properties. The thermal conductivities of $Ln_2Zr_2O_7$ (Ln = La, Nd, Sm, Eu, Gd, Dy, etc) ceramics range from 1.1 to 1.2 W/m·K, which are lower than that of YSZ (Ref 4, 7–9). Because of their promising thermophysical properties, efforts have also been made to investigate the co-doped $Ln_2Zr_2O_7$ ceramics with one or more metal oxides in recent years (Ref 4, 10–13). However, they have relative low coefficients of thermal expansion (CTEs) resulting in high thermal stress in TBC applications, which is harmful for TBC's performance (Ref 14–16).

It is well known that CeO_2 has high thermal expansion coefficient because of its lower melting point compared to ZrO_2, which indicates that the thermal expansion coefficient may be improved by the substitution of CeO_2 for ZrO_2. That is, the $Ln_2Ce_2O_7$ (Ln represents rare earth elements, too) ceramics may have larger thermal expansion coefficients than corresponding $Ln_2Zr_2O_7$ ceramics. Thermophysical properties of $La_2Ce_2O_7$ and $Nd_2Ce_2O_7$ ceramics have been reported by Qiang et al. Results show that thermal conductivities of $La_2Ce_2O_7$ and $Nd_2Ce_2O_7$ are lower than that of YSZ, while their thermal expansion coefficients are higher than that of $La_2Zr_2O_7$ and $Nd_2Zr_2O_7$ ceramics. Moreover, they also show better phase stability at high temperatures (Ref 17, 18). These properties indicate sufficiently that $La_2Ce_2O_7$ and $Nd_2Ce_2O_7$ can be explored as new thermal barrier coating materials. Patwe et al.'s research (Ref 19) results show that thermal expansion coefficient of $Gd_2Ce_2O_7$ is 13.8×10^{-6}/K, which is greater than that of $Gd_2Zr_2O_7$ (11.6×10^{-6}/K). However, $Dy_2Ce_2O_7$ ceramic for thermal barrier coatings has not been investigated up to now. In this research, $Dy_2Ce_2O_7$ ceramic was synthesized by solid state reaction and the microstructure and thermal conductivity of this ceramic were examined.

2. Experimental

Samples of $Dy_2Ce_2O_7$ were synthesized by means of the solid state reaction method, using CeO_2 (Rare-Chem Hi-Tech Co., Ltd, Hui zhou, Guangdong, China, purity ≥ 99.99), Dy_2O_3 (Rare-Chem Hi-Tech Co., Ltd, purity ≥ 99.99%) as the starting materials. After mixing the constituents thoroughly in an agate mortar, the powder mixtures were calcined at 800 °C for 5 h in air. Then the powders were uniaxially cold

Zhang Hongsong, Department of Mechanical Engineering, Henan Institute of Engineering, Zhengzhou 451191, China and School of Material Science and Engineering, Zhengzhou University, Zhengzhou 450007, China; **Liao Suran**, Department of Materials and Chemistry, Henan Institute of Engineering, Zhengzhou 451191, China; and **Guan Shaokang**, School of Material Science and Engineering, Zhengzhou University, Zhengzhou 450007, China. Contact e-mails: zhsandchen@126.com, bitsrliao@126.com, and shaokangguan@126.com.

pressed into pellets, and the pellets were placed on cerium tiles and sintered at 1600 °C for 10 h. The pellets were subsequently cooled in air from 1600 °C in the end.

Phase composition analysis of the synthesized samples were determined by x-ray diffractometry (XRD, X'Pert PRD MPD Holand) with Ni filtered CuKα radiation (0.1542 nm) at the scanning rate of 4°/min. The morphology of fractured cross sections was analyzed using scanning electron microscope (SEM, HITACHI S-4800).

The thermal diffusivities (λ) of synthesized samples were measured using laser-flash method (Model FlashLine^{TM}3000, Anter USA) in the range between ambient and 800 °C in an argon atmosphere. The sample dimension for thermal diffusivity measurement was about 12.7 mm in diameter and about 1 mm in thickness. Before thermal diffusivity measurement, both the front and the back faces of the samples were coated with a thin layer of graphite. These coatings were done to prevent direct transmission of laser beam through the translucent specimens. The thermal diffusivity measurement of the specimens was carried out three times at 200, 400, 600, and 800 °C, respectively. The specific heat capacity (C_p) as a function of temperature was calculated from the heat capacity data of the constituent oxides of $Dy_2Ce_2O_7$, in conjunction with the Neumann–Kopp rule (Ref 20, 21). The thermal conductivity (k) of the specimen was calculated by Eq 1 with specific heat capacity (C_p), density (ρ), and thermal diffusivity (λ).

$$k = \lambda \cdot \rho \cdot C_p \qquad \text{(Eq 1)}$$

Because the sintered specimen was not full dense, the measured values of thermal conductivities were modified for the actual value k_0 using Eq 2, where ϕ is the fractional porosity and the coefficient 4/3 is used to eliminate the effect of porosity on actual thermal conductivity (Ref 22).

$$k/k_0 = 1 - \frac{4}{3}\phi \qquad \text{(Eq 2)}$$

3. Results and discussion

3.1 XRD

The XRD pattern of $Dy_2Ce_2O_7$ prepared by solid reaction is shown in Fig. 1. Figure 1 indicates that the XRD pattern of the prepared ceramic is coincident with the standard spectrum of $Dy_2Ce_2O_7$ and no other phases exist in this product. It is well known that there are two kinds of crystal structure of $A_2B_2O_7$ oxides, which are pyrochlore structure and fluorite structure, respectively. There are two additional weak peaks between 2θ = 40° and 50° in XRD patterns of pyrochlore structure, which can help us to distinguish the fluorite and pyrochlore structures (Ref 17). Early research results revealed that the ionic radius ratio, RR = $\left(r_A^{3+}/r_B^{4+}\right)$ of oxides with the type of $A_2^{3+}B_2^{4+}O_7$, and the oxygen parameter (x) govern the formation and phase stability of these oxides. Pyrochlore oxides can form for RR = 1.46 to 1.78 at one atmosphere, and fluorite oxides will form if RR is lower than 1.46 (Ref 23, 24). The value of RR of $Dy_2Ce_2O_7$ is only 0.94, which also indicate that the synthesized sample has fluorite structure. It can be concluded that pure $Dy_2Ce_2O_7$ ceramics with fluorite structure are synthesized in this research according to the XRD results and the value of RR.

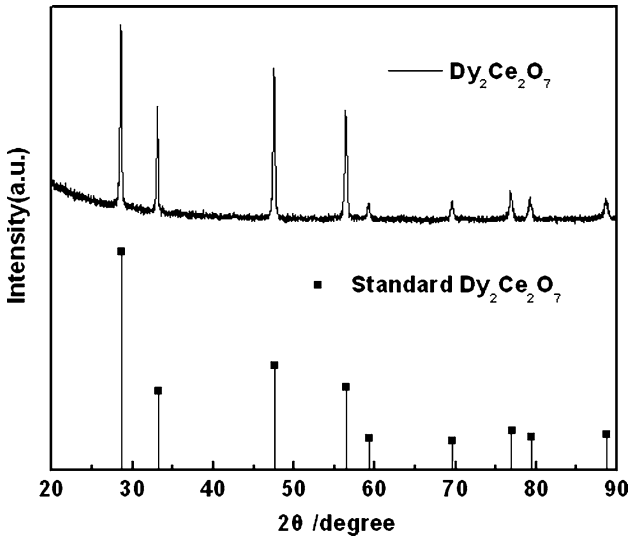

Fig. 1 XRD pattern of $Dy_2Ce_2O_7$

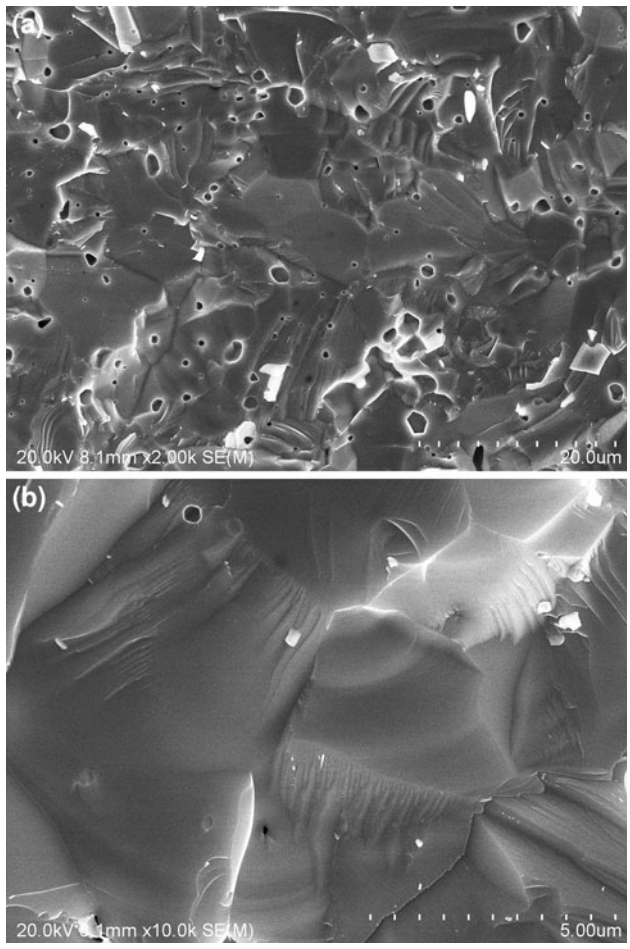

Fig. 2 Microstructure of $Dy_2Ce_2O_7$

3.2 SEM

Figure 2 shows the typical microstructure of $Dy_2Ce_2O_7$ prepared by solid reaction synthesis. As can be seen from Fig. 2(a), its microstructure is very dense, but some apparent pores were found. The density of the sample determined by

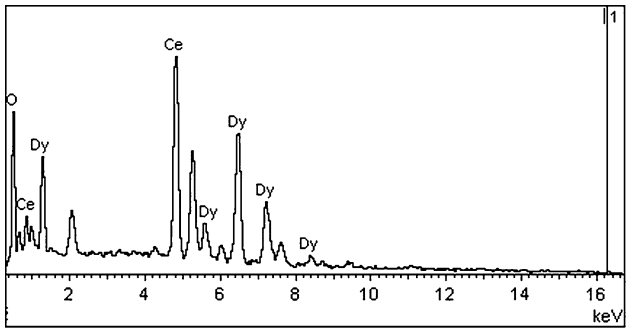

Fig. 3 EDS pattern of $Dy_2Ce_2O_7$

Table 1 Element atomic ratio of $Dy_2Ce_2O_7$

Element	Dy	Ce	O
Atomic ratio (%)	17.67	18.66	63.67

Archimedes method with an immersion medium of deionized water is 7.558 g/cm^3, the relative density of $Dy_2Ce_2O_7$ ceramic sample is 98.8%. Figure 2(b) showed a high-magnification scanning electron micrograph of the $Dy_2Ce_2O_7$ ceramic. It was observed that the interfaces between particles were very clean and no other interphases or unreacted oxides existed in the interfaces, which is shown in Fig. 2(b). The EDS microanalysis pattern in Fig. 3 performed on selected area revealed the presence of mixed oxide phases for Dy-Ce-O. The results of element atomic ratios of these prepared products are displayed in Table 1. As can be seen from Table 1 that the element atomic ratios are consistent with the stoichiometry ratios making up to $Dy_2Ce_2O_7$. Results of EDS analysis displayed in Fig. 3 and Table 1 also imply that pure $Dy_2Ce_2O_7$ ceramic was synthesized successfully which is consistent with XRD pattern of $Dy_2Ce_2O_7$.

3.3 Thermal Conductivity

The specific heat capacity of $Dy_2Ce_2O_7$ ceramic at different temperatures is illustrated in Fig. 4, which indicates that the specific heat capacity increases gradually with temperature increasing. The specific heat capacity can be fitted as the following equation.

$$C_p(Dy_2Ce_2O_7) = 0.35991 + 0.0001 \times T - 55.25098 \times T^{-2} \quad \text{(Eq 3)}$$

The thermal diffusivity of $Dy_2Ce_2O_7$ ceramic decreases with increasing of temperature in the range between ambient temperature and 800 °C, i.e., $\lambda \propto T^{-1}$, which is plotted in Fig. 5. The dependence of thermal diffusivity on temperature in this temperature range suggests a dominant phonon conduction behavior, which resembles most polycrystalline materials. The thermal conductivity of $Dy_2Ce_2O_7$ ceramic is thus obtained according to Eq 1, and the result is shown in Fig. 6. It can be seen from Fig. 6 that the thermal conductivity of $Dy_2Ce_2O_7$ decreases gradually with temperature increasing. The value of thermal conductivity decreases from 2.63 to 1.78 W/m·K and the thermal conductivity of $Dy_2Ce_2O_7$ at 800 °C is almost lower 20% than that of YSZ (about 2.15 W/m·K at 800 °C). It is well known that thermal conductivity of CeO_2 is higher than

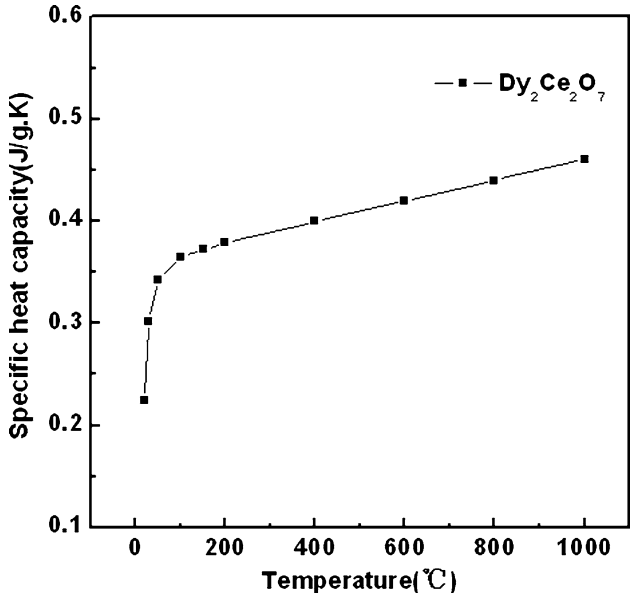

Fig. 4 Specific heat capacity of $Dy_2Ce_2O_7$

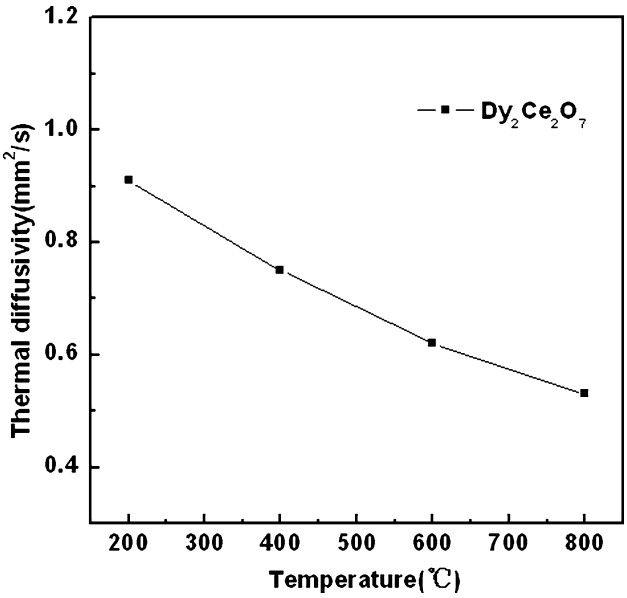

Fig. 5 Thermal diffusivity of $Dy_2Ce_2O_7$ as a function of temperature

that of YSZ at temperatures below 1300 °C (2.77 W/m·K at 1000 °C). The lower thermal conductivity of $Dy_2Ce_2O_7$ can be explained in light of phonon theory.

To rationalize this result, the theory of heat conduction is considered. In electrical insulating solids, the thermal conductivity results from lattice vibrations or by radiation. The contribution to thermal conductivity from lattice vibration (k), the quanta of which are known as phonons, is given by:

$$k = \frac{1}{3} C_v l_p \rho v \quad \text{(Eq 5)}$$

where C_v is the specific heat capacity, ρ is the density, v is the phonon velocity, and l_p is the mean free path for scattering of phonons.

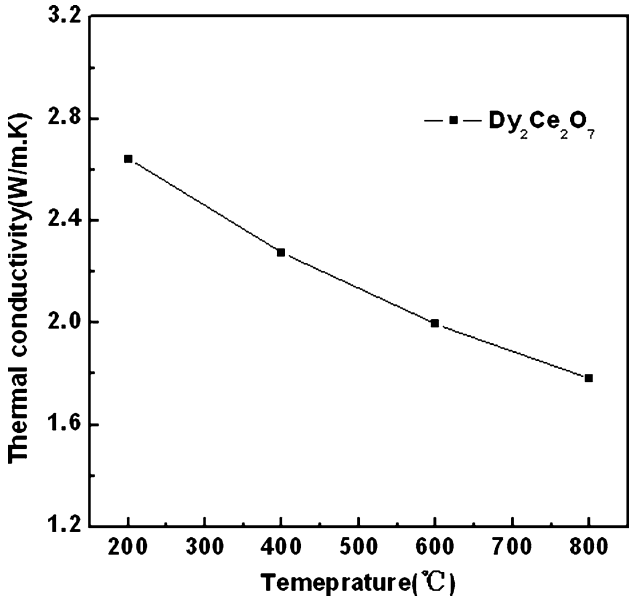

Fig. 6 Dependence of thermal conductivity of $Dy_2Ce_2O_7$ on temperature

To reduce the intrinsic thermal conductivity of a material, reductions in the specific heat capacity, phonon velocity, mean free path, or density are needed. The specific heat capacity at constant volume (C_v) for any system is constant at a value of $3\,\text{kbN} \approx 25\,\text{J/K} \cdot \text{mol}$ above the Debye temperature. The value of v is related with elastic ratio (E) and density (ρ), the effect of temperature on the elastic ratio and density is not obvious, so the value of v may be also regarded as a constant approximately. Consequently, the value of the thermal conductivity (k) is mainly decided by the law that the mean free path of phonon decreases with increasing temperature among most polycrystalline ceramic materials. In real crystal structures scattering of phonons occurs when they interact with lattice imperfections in the ideal lattice. Such imperfections include vacancies, dislocations, grain boundaries, atoms of different masses and other phonons. Ions and atoms of different ionic radius may also scatter phonons by locally distorting the bond length and thus, introducing elastic strain fields into the lattice. The effects caused by such imperfections can be quantified through their influence on the phonon mean free path (l_p). This approach has been used by many workers, for which the phonon mean free path is defined by:

$$\frac{1}{l_p} = \frac{1}{l_i} + \frac{1}{l_{vac}} + \frac{1}{l_{gb}} + \frac{1}{l_{strain}} \qquad \text{(Eq 6)}$$

where l_i, l_{vac}, l_{gb}, and l_{strain} are the contributions to the mean path due to interstitials, vacancies, grain boundaries and lattice strain, respectively (Ref 25).

The decrease of the thermal conductivity due to the phonon scattering at grain boundaries is not expected in the case of the ceramic material investigated here. For a significant decrease in the high-temperature range, the average grain size has to be in the nanometer region, whereas the current specimen has grain size in the micrometer range. Also, radiation heat transfer can be neglected because the maximum temperature considered here is only 800 °C. Thus, the decrease in the phonon conductivity is assumed to result mainly from phonon scattering by point defect. The two types of point defects expected in the materials studied here are substitutional dysprosium solute cation replacing cerium and the corresponding oxygen vacancies created by the substitution of tetravalent cerium by a trivalent dysprosium cation. The defect chemistry due to co-doping can be represented using the Kröger–Vink notation by the following equation,

$$Dy_2O_3 \xrightarrow{CeO_2} 2Dy'_{Ce} + V''_o + 3O^x_o \qquad \text{(Eq 7)}$$

where Dy'_{Ce} represents an Dy^{3+} cation that occupies a Ce^{4+} cation site (single negative charge), V''_o is a doubly charged (positive) oxygen vacancy, and O^x_o is an O^{2-} anion on an oxygen site (neutral charge). The electric charges are defined with respect to the pure CeO_2 lattice. Equation 7 shows that the higher the content of Dy_2O_3 is, the more oxygen vacancies are created. The content of Dy_2O_3 is 33 mol% in $Dy_2Ce_2O_7$, while that of Y_2O_3 is only 4.02 mol% in 8YSZ. Clearly, the concentration of oxygen vacancies in $Dy_2Ce_2O_7$ is significant higher than that in 8YSZ. Therefore, the thermal conductivity of $Dy_2Ce_2O_7$ is lower than that of 8YSZ due to the scattering of the phonons by the oxygen vacancies.

In addition to the phonon scattering by the oxygen vacancies, another reason of low thermal conductivity of $Dy_2Ce_2O_7$ is the scattering of phonons by the substitutional cation. $Dy_2Ce_2O_7$ is a solid solute of Dy_2O_3 in CeO_2. For substitutional atoms existing in the lattice of oxides, the mean free path of phonon l_p is given by (Ref 9),

$$\frac{1}{l_p} = \frac{a^3}{4\pi v^4}\omega^4 c\left(\frac{\Delta M}{M}\right)^2 \qquad \text{(Eq 5)}$$

where a^3 is the volume per atom, v the transverse wave speed, ω the phonon frequency, c the concentration per atom, M is the average mass of the host atom, $M + \Delta M$ is the average mass of the solute atom. Equation 5 shows that the phonon mean free path is proportional to the square of the atomic weight difference between the solute and host (Ce) cations. Because atomic weight of Cerium and dysprosium is 141.2 and 162.5, respectively, the effective phonon scattering by Dy^{3+} solute cations also contributes to the lower thermal conductivity of $Dy_2Ce_2O_7$. Because of higher atom weight difference between dysprosium (162.5) and zirconium (91) in $Dy_2Zr_2O_7$, the effective phonon scattering in $Dy_2Zr_2O_7$ is slightly higher than that in $Dy_2Ce_2O_7$, which contributes to a lower thermal conductivity of $Dy_2Zr_2O_7$ compared to $Dy_2Ce_2O_7$. However, the thermal conductivity of $Dy_2Ce_2O_7$ still meets the basic requirement for TBCs. It is well known that low thermal conductivity is one of the most critical requirements for TBCs (Ref 26). The lower thermal conductivity of $Dy_2Ce_2O_7$ indicates that this ceramic material can be explored as novel candidate prospective ceramic materials for use in TBCs.

4. Conclusions

Single-phase $Dy_2Ce_2O_7$ with fluorite structure was synthesized by solid state reaction between Dy_2O_3, CeO_2 powders at 1600 °C for 10 h. Thermal conductivity of $Dy_2Ce_2O_7$ ceramic materials is lower than that of 8YSZ which means this ceramic can be explored as novel candidate ceramic materials for use in TBCs. The lower thermal conductivity can be attributed to the

significant higher concentration of oxygen vacancies and the significantly larger atomic weight difference of the solute cations in this material.

Acknowledgments

This study is supported by the Doctor Research Fund (D2007012), and the program for innovative research team (in science and technology) (2009IRTHNIE05) of Henan Institute of Engineering.

References

1. N.P. Padture, M. Gell, and E.H. Jordan, Thermal Barrier Coatings for Gas-Turbine Engine Applications, *Science*, 2002, **12**, p 280–284
2. G.W. Goward, Progess in Coatings for Gas Turbine Airfoils, *Surf. Coat. Technol.*, 1998, **108–109**, p 73–79
3. T.M. Yonushonis, Overview of Thermal Barrier Coatings in Diesel Engines, *J. Thermal. Spray. Technol.*, 1997, **3**, p 50–56
4. D. Hui, Z.X. Hua, L.J. Yan, Z.Y. Fei, M. Jian, and C.X. Qiang, Thermal Stability of Double-Ceramic-Layer Thermal Barrier Coatings with Various Coating Thickness, *Mater. Sci. Eng.*, 2006, **A433**, p 1–7
5. J.Y. Li, H. Dai, X.H. Zhang, Y.F. Zhang, X.F. Ma, J. Meng, and X.Q. Cao, Lanthanum Zirconate Ceramic Toughened by $BaTiO_3$ Secondary Phase, *J. Alloy. Compd.*, 2008, **452**, p 406–409
6. Z.G. Liu, J.H. Ouyang, and Y. Zhou, Preparation and Thermophysical Properties of $(Nd_xGd_{1-x})_2Zr_2O_7$ Ceramics, *J. Mater. Sci.*, 2008, **43**, p 3596–3603
7. R. Terki, G. Bertrand, H. Aourag, and C. Coddet, Thermal Properties of $Ba_{1-x}Sr_xZrO_3$ Compounds for Microscopic Theory, *J. Alloy. Compd.*, 2008, **456**, p 508–513
8. H. Lehmann, D. Pitzer, G. Pracht, R. Vassen, and D. Stover, Thermal Conductivity and Thermal Expansion Coefficients of the Lanthanum Rare-Earth-Element Zirconates, *J. Am. Soc.*, 2003, **86**(8), p 1338–1344
9. Q. Xu, W. Pan, J.D. Wang, L.H. Qi, H.Z. Miao, and T. Kazutaka, Tortigoe, Preparation and Thermophysical Properties of $Dy_2Zr_2O_7$ Ceramic for Thermal Barrier Coatings, *Mater. Lett.*, 2005, **59**, p 2804–2807
10. J. Wang, S.X. Bai, H. Zhang, and C.R. Zhang, The Structure Thermal Expansion Coefficient and Sintering Behavior of Nd^{3+} Doped $La_2Zr_2O_7$ for Thermal Barrier Coatings, *J. Alloy. Compd.*, 2009, **476**, p 89–91
11. Z.G. Liu, J.H. Ouyang, Y. Zhou, J. Li, and X.L. Xia, Influence of Yttrium and Samarium Oxides Codoping on Structure and Thermal Conductivity of Zirconate Ceramics, *J. Eur. Ceram. Soc.*, 2009, **29**, p 647–652
12. H.S. Zhang, Q. Xu, F.C. Wang, L. Liu, Y. Wei, and X.G. Chen, Preparation and Thermophysical Properties of $(Sm_{0.5}La_{0.5})_2Zr_2O_7$ and $(Sm_{0.5}La_{0.5})_2(Zr_{0.8}Ce_{0.2})_2O_7$ Ceramics for Thermal Barrier Coatings, *J. Alloy. Compd.*, 2009, **475**, p 624–628
13. H.S. Zhang, K. Sun, Q. Xu, F.C. Wang, and L. Liu, Thermal Conductivity of $(Sm_{1-x}La_x)_2Zr_2O_7$ (x = 0, 0.25, 0.5, 0.75 and 1) Oxides for Advanced Thermal Barrier Coating, *J. Rare Earth*, 2009, **27**, p 222–226
14. Z.H. Xu, L.M. He, X.H. Zhong, R.D. Mu, S.M. He, and X.Q. Cao, Thermal Barrier Coatings of Lanthanum-Zirconate Cerium Composite Oxide Made by Electron Beam Physical Vapor Deposition, *J. Alloy. Compd.*, 2009, **478**, p 168–172
15. H.F. Chen, Y.F. Gao, S.Y. Tao, Y. Liu, and H.J. Luo, Coprecipitation Synthsis and Thermal Conductivity of $La_2Zr_2O_7$, *J. Alloys Compd.*, 2009, **486**, p 391–396
16. Z.H. Xu, L.M. He, R.D. Mu, G.H. Huang, and X.Q. Cao, Double Ceramic Layer Thermal Barrier Coatings Based on $La_2(Zr_{0.7}Ce_{0.3})_2O_7$/$La_2Ce_2O_7$ Deposited by Eletron Beam Physical Vapor Deposition, *Appl. Surf. Sci.*, 2010, **256**, p 3661–3668
17. C.X. Qiang, R. Vassen, W. Fischer, F. Tietz, and D. Stover, Lanthanum-cerium Oxides as Thermal Barrier-coating Materials for High-temperature Applications, *Adv. Mater.*, 2003, **9**, p 1438–1442
18. H. Dai, X.H. Zhong, J.Y. Li, J. Meng, and X.Q. Cao, Neodymium-cerium Oxides as New Thermal Barrier Coatings Material, *Surf. Coat. Technol.*, 2006, **201**, p 2527–2533
19. S.J. Patwe, B.R. Ambekar, and A.K. Tyagi, Synthesis, Characterization and Lattice Thermal Expansion of Some Compounds in the System $Gd_2Ce_xZr_{2-x}O_7$, *J. Alloy. Compd.*, 2005, **389**, p 243–246
20. P.G. Spencer, Estimation of Thermodynamic Data for Metallurgical Applications, *Thermochim. Acta*, 1999, **314**, p 1–21
21. J.D. Leitner, P. Chuchvalec, and D. Sedmidubsky, Estimation of Heat Capacity of Solid Mixed Oxides, *Thermochim. Acta*, 2003, **395**, p 27–46
22. N.P. Bansal and Z.D. Ming, Effects of Doping on Thermal Conductivity of Pyrochlore Oxides for Advanced Thermal Barrier Coatings, *Mater. Sci. Eng.*, 2007, **A459**, p 192–195
23. M.A. Subramanian, G. Aravamudan, and G.V.S. Rao, Oxides Pyrochlore—A Review, *Prog. Solid State Chem.*, 1983, **15**, p 55–143
24. X.L. Xia, J.H. Ouyang, and Z.G. Liu, Influence of Cao on Structure and Electrical Conductivity of Pyrochlore-type $Sm_2Zr_2O_7$, *J. Power Sour.*, 2009, **189**, p 888–893
25. J.R. Nicholls, K.J. Lawson, A. Johnstone, and D.S. Rickerby, Methods to Reduce the Thermal Conductivity of EB-PVD TBCs, *Surf. Coat. Technol.*, 2002, **151–152**, p 381–391
26. S. Yamanaka, T. Maekawa, H. Muta, T. Matsuda, S. Kobayshi, and K. Kurosaki, Thermal and Mechanical Properties of $SrHfO_3$, *J. Alloy. Compd.*, 2004, **381**, p 295–300